

# Two-dimensional composite solitons in Bose-Einstein condensates with spatially confined spin-orbit coupling

Yogyao Li<sup>1</sup>, Zhihuan Luo<sup>2</sup>, Chunqing Huang<sup>1</sup>, Wei Pang<sup>3,\*</sup> and Boris A. Malomed<sup>4,1</sup>

<sup>1</sup>*School of Physics and Optoelectronic Engineering, Foshan University, Foshan 528000, China*

<sup>2</sup>*College of Electronic Engineering, South China Agricultural University,*

*Guangzhou 510642, China*

<sup>3</sup>*Department of Experiment Teaching,*

*Guangdong University of Technology, Guangzhou 510006, China*

<sup>4</sup>*Department of Physical Electronics, School of Electrical Engineering, Faculty of Engineering, and Center for Light-Matter Interaction, Tel Aviv University, Tel Aviv 69978, Israel*

It was recently found that the spin-orbit (SO) coupling can help to create stable matter-wave solitons in spinor Bose-Einstein condensates in the two-dimensional (2D) free space. Being induced by external laser illumination, the effective SO coupling can be applied too in a spatially confined area. Using numerical methods and the variational approximation (VA), we build families of 2D solitons of the semi-vortex (SV) and mixed-mode (MM) types, and explore their stability, assuming that the SO-coupling strength is confined in the radial direction as a Gaussian. The most essential result is identification, by means of the VA and numerical methods, of the minimum size of the spatial confinement for which the 2D system maintains stable solitons of the SV and MM types.

## I. INTRODUCTION

Many-body self-trapping has been drawing much interest in studies of atomic Bose-Einstein condensates (BECs). In particular, creation of stable two- and three-dimensional (2D and 3D) solitons in is a challenging issue, as the usual cubic self-attraction destabilizes all formally available multidimensional solitons due to the possibility of the collapse [1, 2]. Two schemes were theoretically elaborated to solve the stability problem for matter-wave solitons in the 2D and 3D free space. One is the use of nonlocal nonlinearity, which may be induced by the Van der Waals interactions between Rydberg atoms [3], dipole-dipole interactions between atoms or molecules carrying magnetic or electric dipolar moments [4–6], or the microwave-mediated local field effect in spinor BECs [7]. The second scheme relies upon the beyond-mean-field corrections, induced by quantum fluctuations, add the Lee-Huang-Yang (LHY) terms to the underlying Gross-Pitaevskii equations (GPEs). The latter approach has made it possible to theoretically predict [9]–[11] and experimentally create self-trapped “quantum droplets”, in dipolar [12–14] and binary BECs [15–17].

Recently, an unexpected result was reported, predicting a possibility to create absolutely stable (ground-state) and metastable matter-wave solitons in the 2D [18] and 3D [19] free space, respectively, with the help of the spin-orbit (SO) coupling, which can be induced in binary (pseudo-spinor) BEC by means of appropriate laser fields, see original works [20]–[22] and reviews [23]–[25]. While a majority of experimental works aimed to create the SO coupling in effectively 1D settings, an experimental realization of an effectively 2D SO coupling was reported too [26, 27]. In the setting considered in Ref. [18], the SO coupling can protect 2D solitons against collapsing, creating a ground state [29], which is otherwise missing in 2D GPEs with the cubic self-attraction [30]–[32]. The collapse remains possible in the presence of SO coupling, starting with the norm of the input which exceeds the threshold value for the onset of the 2D collapse. Similar settings can be implemented in optics, predicting the creation of spatiotemporal solitons (“light bullets”) in planar dual-core waveguides with the self-focusing Kerr nonlinearity [33, 34]. Further, the interplay between the SO coupling and anisotropic dipole-dipole interactions in 2D free space can create stripe solitons [35], solitary vortices [36], and gap solitons [37] (2D free-space gap solitons can also be created in SO-coupled BECs with contact interactions, at appropriate values of parameters [38]). Recently, it was also found that the combination of LHY and SO-coupling terms in 2D creates anisotropic “quantum droplets” in spinor BECs [11].

Previous works on 2D and 3D solitons in SO-coupled BECs tacitly assumed that the SO-couplings was applied homogeneously in the entire space. Because this effect is engineered by applied laser fields, it can be applied in a spatially confined area. This possibility was analyzed, in the framework of the 1D SO-coupling model, in Ref. [39]. While stable 1D matter-wave solitons can be created without the use of the SO coupling [40]–[42], [43], the analysis reported in Ref. [39] has revealed new possibilities, such as the creation of stable two-soliton bound states. The purpose of the present work is to construct 2D solitons supported by spatially confined SO coupling, which is a challenging issue, as 2D solitons are unstable without the SO coupling. Thus, in particular, a relevant problem is

---

\*Electronic address: kingprotoss@gmail.com

to identify the minimum area carrying the SO coupling which is necessary to maintain the solitons' stability. We address this problem, assuming an isotropic shape of the spatial modulation of the local SO strength, with a Gaussian dependence on the radial coordinate. The results are obtained by means of an analytical variational approximation (VA) and systematic numerical calculations. The rest of the paper is structured as follows: the model and VA are introduced in Sections II and III, respectively, and numerical results, including their comparison with predictions of the VA are summarized in Section IV. The paper is concluded by Sec. V.

## II. THE MODEL

As said above, we consider the binary BECs, with a pseudo-spinor wave function  $(\phi_+, \phi_-)$ , whose components are SO-coupled in a finite 2D area. The mean-field model of this system is based on the Lagrangian,

$$\mathcal{L} = \int \int \mathcal{L} dx dy, \quad (1)$$

$$\begin{aligned} \mathcal{L} = & -\frac{i}{2} \left( \phi_+^* \frac{\partial \phi_+}{\partial t} + \phi_-^* \frac{\partial \phi_-}{\partial t} + \text{c.c.} \right) \\ & + \frac{1}{2} \left( |\nabla \phi_+|^2 + |\nabla \phi_-|^2 \right) - \frac{1}{2} (|\phi_+|^4 + |\phi_-|^4) - \gamma |\phi_+|^2 |\phi_-|^2 \\ & + \frac{\lambda(r)}{2} \left\{ \left[ \phi_+^* \frac{\partial \phi_-}{\partial x} - \phi_-^* \frac{\partial \phi_+}{\partial x} - i \left( \phi_+^* \frac{\partial \phi_-}{\partial y} + \phi_-^* \frac{\partial \phi_+}{\partial y} \right) \right] + \text{c.c.} \right\}. \end{aligned} \quad (2)$$

where c.c. stands for the complex conjugate expression. The SO coupling of the Rashba type is accepted here, with a strength confined to values of the radial coordinate  $r \lesssim L$ :

$$\lambda(r) = \lambda_0 \exp(-r^2/L^2), \quad (3)$$

where and  $\lambda_0 \equiv 1$  may be fixed by means of rescaling. Further,  $\gamma$  is the relative strength of the cross attraction, while the strength of the self-attraction is normalized to be 1. The Hamiltonian corresponding to Lagrangian (1) is

$$\begin{aligned} E = & \int \int (\mathcal{E}_K + \mathcal{E}_N + \mathcal{E}_{SOC}) dx dy, \\ \mathcal{E}_K = & \frac{1}{2} (|\nabla u_+|^2 + |\nabla u_-|^2), \quad \mathcal{E}_N = -\frac{1}{2} (|u_+|^4 + |u_-|^4) - 2\gamma |u_+|^2 |u_-|^2, \\ \mathcal{E}_{SOC} = & \frac{\lambda(r)}{2} \left\{ \left[ u_+^* \left( \frac{\partial u_-}{\partial x} - i \frac{\partial u_-}{\partial y} \right) - u_-^* \left( \frac{\partial u_+}{\partial x} + i \frac{\partial u_+}{\partial y} \right) \right] + \text{c.c.} \right\}, \end{aligned} \quad (4)$$

where  $\mathcal{E}_{K,N,SOC}$  are densities of kinetic, interaction, and SO-coupling energies, respectively.

The GPE system is derived from Lagrangian (1) as the Euler-Lagrange equations, written here in polar coordinates  $(r, \theta)$ , as suggested by the fact that  $\lambda$  is defined as a function of  $r$  in Eq. (3) [the following relations are useful in this context:  $\frac{\partial}{\partial x} - i \frac{\partial}{\partial y} \equiv e^{-i\theta} \left( \frac{\partial}{\partial r} - \frac{i}{r} \frac{\partial}{\partial \theta} \right)$ ,  $\frac{\partial}{\partial x} + i \frac{\partial}{\partial y} \equiv e^{i\theta} \left( \frac{\partial}{\partial r} + \frac{i}{r} \frac{\partial}{\partial \theta} \right)$ ],

$$\begin{aligned} i \frac{\partial \phi_+}{\partial t} &= -\frac{1}{2} \nabla^2 \phi_+ - (|\phi_+|^2 + \gamma |\phi_-|^2) \phi_+ + \lambda(r) e^{-i\theta} \left( \frac{\partial \phi_-}{\partial r} - \frac{i}{r} \frac{\partial \phi_-}{\partial \theta} \right) + \frac{1}{2} e^{-i\theta} \frac{d\lambda}{dr} \phi_-, \\ i \frac{\partial \phi_-}{\partial t} &= -\frac{1}{2} \nabla^2 \phi_- - (|\phi_-|^2 + \gamma |\phi_+|^2) \phi_- - \lambda(r) e^{i\theta} \left( \frac{\partial \phi_+}{\partial r} + \frac{i}{r} \frac{\partial \phi_+}{\partial \theta} \right) - \frac{1}{2} e^{i\theta} \frac{d\lambda}{dr} \phi_+. \end{aligned} \quad (5)$$

Note that the last terms in Eq. (5), produced by the  $r$ -dependence of  $\lambda$ , may be considered as a specific form of the Rabi coupling.

Stationary solutions to Eq. (5) with chemical potential  $\mu$  are looked for as

$$\{\phi_{\pm}(x, y, t)\} = e^{-i\mu t} u_{\pm}(x, y), \quad (6)$$

where functions  $u_{\pm}$  satisfy equations

$$\begin{aligned} \mu u_+ &= -\frac{1}{2} \nabla^2 u_+ - (|u_+|^2 + \gamma |u_-|^2) u_+ + \lambda(r) e^{-i\theta} \left( \frac{\partial u_-}{\partial r} - \frac{i}{r} \frac{\partial u_-}{\partial \theta} \right) + \frac{1}{2} e^{-i\theta} \frac{d\lambda}{dr} u_-, \\ \mu u_- &= -\frac{1}{2} \nabla^2 u_- - (|u_-|^2 + \gamma |u_+|^2) u_- - \lambda(r) e^{i\theta} \left( \frac{\partial u_+}{\partial r} + \frac{i}{r} \frac{\partial u_+}{\partial \theta} \right) - \frac{1}{2} e^{i\theta} \frac{d\lambda}{dr} u_+, \end{aligned} \quad (7)$$

which can be derived from their own Lagrangian density:

$$\begin{aligned} \mathcal{L}_{\text{stat}} = & -\mu \left( |u_+|^2 + |u_-|^2 \right) + \frac{1}{2} \left( |\nabla u_+|^2 + |\nabla u_-|^2 \right) - \frac{1}{2} (|u_+|^4 + |u_-|^4) - \gamma |u_+|^2 |u_-|^2 \\ & + \frac{\lambda(r)}{2} \left\{ \left[ e^{-i\theta} u_+^* \left( \frac{\partial u_-}{\partial r} - \frac{i}{r} \frac{\partial u_-}{\partial \theta} \right) - e^{i\theta} u_-^* \left( \frac{\partial u_+}{\partial r} + \frac{i}{r} \frac{\partial u_+}{\partial \theta} \right) \right] + \text{c.c.} \right\}. \end{aligned} \quad (8)$$

### III. SEMI-VORTICES (SVS) AND THE VARIATIONAL APPROXIMATION (VA) FOR THEM

Equations (7) admit solutions in the form of a *semi-vortex* (SV):

$$u_+ = f(r), \quad u_- = \exp(i\theta) rg(r), \quad (9)$$

with  $\mu < 0$ . This ansatz is exactly compatible with Eq. (7), but real functions  $f(r)$  and  $g(r)$  must be found numerically. They exponentially decay  $\sim \exp(-\sqrt{-2\mu}r)$  at  $r \rightarrow \infty$  [note that  $\lambda(r)$  vanishes at  $r \rightarrow \infty$ , hence the SO-coupling does not affect the asymptotic form at  $r \rightarrow \infty$ ], and take finite values,  $f(r=0) \neq 0$  and  $g(r=0) \neq 0$ , at  $r=0$ , with zero values of the derivatives:  $f'(r=0) = g'(r=0) = 0$ .

The SV may be approximated by the Gaussian variational ansatz, with different amplitudes,  $A$  and  $B$ , and common width  $W$ , cf. Ref. [18]:

$$u_+(r) = A \exp\left(-\frac{r^2}{2W^2}\right), \quad u_-(r) = Br \exp\left(i\theta - \frac{r^2}{2W^2}\right). \quad (10)$$

The substitution of this ansatz in Lagrangian density (8) and spatial integration yields the effective Lagrangian corresponding to the ansatz:

$$\frac{\mathbb{L}}{\pi} = -\mu (A^2 W^2 + B^2 W^4) + \frac{A^2}{2} + B^2 W^2 - \frac{A^4 W^2}{4} - \frac{B^4 W^6}{8} - \frac{\gamma A^2 B^2 W^4}{4} + \frac{2ABL^2 W^2}{L^2 + W^2}, \quad (11)$$

which gives rise to the variational equations,  $\partial L/\partial A = \partial L/\partial B = \partial L/\partial (W^2) = 0$ , i.e.,

$$\begin{aligned} \frac{2L^2 B W^2}{L^2 + W^2} &= 2\mu A W^2 - A + A^3 W^2 + \frac{\gamma}{2} A B^2 W^4, \\ \frac{2L^2 A}{L^2 + W^2} &= 2\mu B W^2 - 2B + \frac{1}{2} B^3 W^4 + \frac{\gamma}{2} A^2 B W^2, \\ \frac{2L^4 A B}{(L^2 + W^2)^2} &= \mu A^2 + 2\mu B^2 W^2 - B^2 + \frac{1}{4} A^4 + \frac{3}{8} B^4 W^4 + \frac{\gamma}{2} A^2 B^2 W^2. \end{aligned} \quad (12)$$

The total norm of ansatz (10) is

$$\begin{aligned} N &= \int [|\phi_+(\mathbf{r})|^2 + |\phi_-(\mathbf{r})|^2] d\mathbf{r} \equiv N_+ + N_- \\ &= \pi (A^2 W^2 + B^2 W^4). \end{aligned} \quad (13)$$

In particular, analysis of Eqs. (12) and (13) reproduces the known fact [18] that, in the uniform space ( $L = \infty$ ), SVs exist with norms falling below a limit value,  $N < N_T$ , where  $N_T$  is the norm of the *Townes' soliton* [1, 2, 44] produced by the single GPE in the 2D setting. The present version of the VA predicts the known approximate value,  $N_T^{(\text{VA})} = 2\pi$  [45], a numerically exact one being  $N_T \approx 5.85$ . Results produced by the VA for VSs are compared to numerical findings in the next section. In particular, the VA predicts the minimum size of the SO-coupling area,  $L_{\text{cr}}$ , necessary for supporting 2D solitons.

### IV. NUMERICAL RESULTS

#### A. Stationary semi-vortices (SVs) and mixed modes (MMs)

According to Ref. [18], two types of 2D solitons, the above-mentioned SVs and mixed modes (MMs), can be produced by the SO-coupled GPEs. It is relevant to mention that, in the uniform space ( $L = \infty$ ), the MMs exist

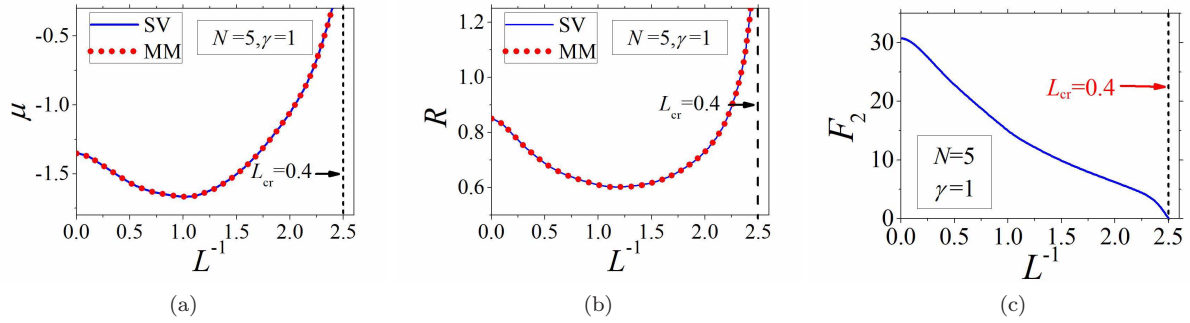


FIG. 1: (Color online) (a,b) Effective radius (17) and the chemical potential of the SVs (blue solid curves) MMs (red dot curves) versus  $L$ . Here we fix  $(N, \gamma) = (5, 1)$ . (c) The vorticity-carrying norm share  $F_2$  of SVs [see Eq. (18)] vs.  $L$ .

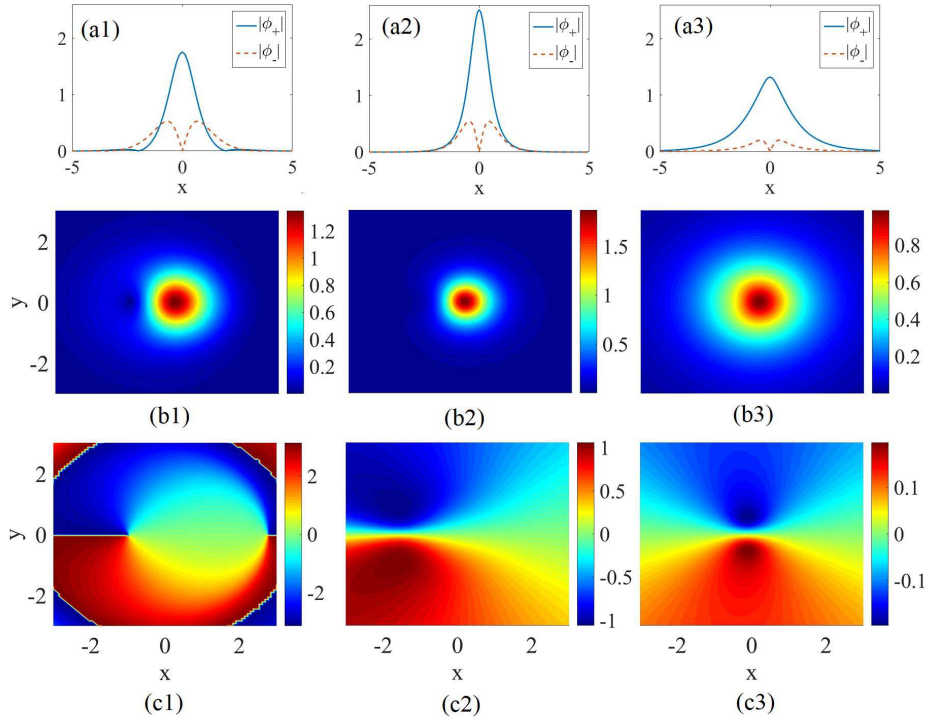


FIG. 2: (Color online) (a1-a3) Amplitude profiles in cross-sections of the fundamental and vortex components (blue solid and red dashed curves, respectively) of stable SVs. (b1-b3) 2D amplitude pattern of component  $\phi_+$  of stable MMs. (c1-c3) The phase patterns of  $\phi_+$  corresponding to panels (b1-b3), respectively. The size of the SO-coupling confinement,  $L$ , from left to right columns is  $L = \infty, 1, 0.41$ , respectively. Other parameters are  $\gamma = 1$  and  $N = 5$ .

with the norm falling below the limit value,

$$N < N_{\text{lim}} = 2(1 + \gamma)^{-1} N_T, \quad (14)$$

where  $N_T$  is the above-mentioned norm of the Townes' soliton, which sets the limit for the SV's norm.

Stationary SVs can be numerically obtained, solving Eq. (5) by means of the imaginary-time method, starting from input

$$\phi_+^{(0)} = A_+ \exp(-\alpha_+ r^2), \quad \phi_-^{(0)} = A_- r \exp(i\theta - \alpha_- r^2), \quad (15)$$

with real constants  $A_{\pm}$  and  $\alpha_{\pm} > 0$ . Note that this input is similar to, but different from variational ansatz (10).

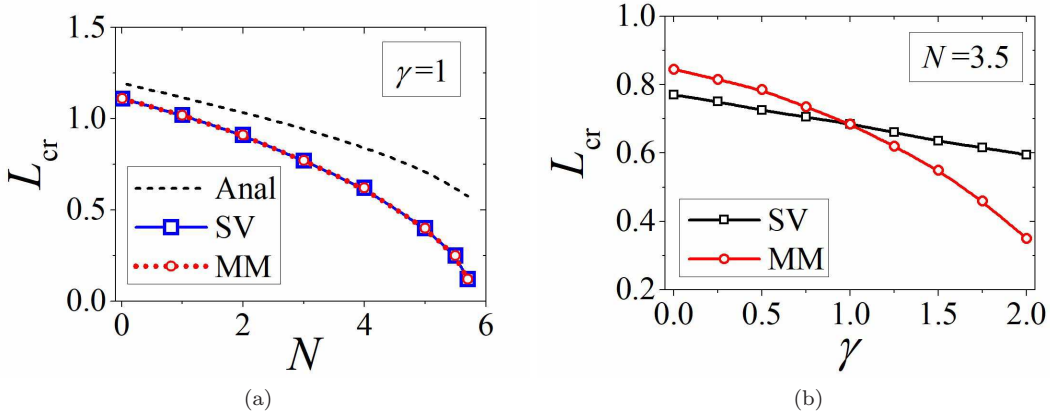


FIG. 3: (Color online) (a)  $L_{\text{cr}}$  of SVs (blue solid with squares) and MMs (red dots with circles) vs.  $N$  at  $\gamma = 1$ . The dashed curve is dependence  $L_{\text{cr}}(N)$  predicted by the VA, see the text. (b)  $L_{\text{cr}}$  of SVs (black squares) and MMs (red circles) vs.  $\gamma$  at  $N = 3.5$ .

Similarly, MMs are produced by the imaginary-time integration initiated by input

$$\phi_{\pm}^{(0)} = A_1 \exp(-\alpha_1 r^2) \mp A_2 r \exp(-\alpha_2 r^2 \mp i\theta), \quad (16)$$

with  $\alpha_{1,2} > 0$ . Unlike Eq. (9), an ansatz built in the form of Eq. (16) is not compatible with Eq. (7). Nevertheless, the general structure represented by the ansatz, i.e., a superposition of vorticities  $(0, +1)$  and  $(0, -1)$  in the two components. is also featured by numerical solutions for the MM.

To address effects of confinement size  $L$  of the SO coupling, which is defined in Eq. (3), we define an effective radius of the soliton, as

$$R = \left( \frac{\int r^2 n(\mathbf{r}) d\mathbf{r}}{\int n(\mathbf{r}) d\mathbf{r}} \right)^{1/2}, \quad (17)$$

where  $n(\mathbf{r}) = |\phi_+(\mathbf{r})|^2 + |\phi_-(\mathbf{r})|^2$  is the total density of the solution. For the SVs, it is also relevant to define the relative share of the total number of atoms which are kept in the vortex component:

$$F_2 = \frac{N_-}{N} \times 100\%, \quad (18)$$

as per definition of  $N_-$  given by Eq. (13). For MMs solutions, norms of their components are always equal. Dependences of these characteristics on  $L$ , obtained from numerical solutions, are produced below, along with results verifying stability of the solitons.

Figures 1(a,b) display the chemical potentials and radii of the SVs and MMs, defined by Eq. (17), for characteristic values of other parameters,  $(N, \gamma) = (5, 1)$ , as functions of the SO-coupling confinement size,  $L$ . Note that the values of  $\mu$  and  $R$  for SVs and MMs are identical for  $\gamma = 1$ , which is a manifestation of the specific degeneracy of the soliton families in this case (in the uniform space, with  $L = \infty$ , the SVs and MMs are limit cases of a broader soliton family with an additional intrinsic parameter; the same may be true in the case of finite  $L$ , which should be a subject for additional analysis). Values of  $\mu(L)$  and  $R(L)$  decrease with  $L$  varying from infinity to  $L \approx 0.83$ , and then increase with the subsequent decrease of  $L$ . This behavior implies that, initially, the solitons undergo self-compression with the reduction of the size of the SO-coupling area, which is changed by expansion. As  $L$  approaches the critical value,  $L_{\text{cr}} \approx 0.4$ , at which the solitons suffer delocalization,  $R(L)$  asymptotically diverges, while  $\mu(L)$  vanishes in the same limit. Solitons do not exist at  $L < L_{\text{cr}}$ . Further, 1(c) shows that the share of the total norm in the vortex component of the SV monotonously decays with the decrease of  $L$ , vanishing in the limit of  $L = L_{\text{cr}}$ . A similar trend occurs for the MMs, in both components of which the vortex terms are vanishing at  $L \rightarrow L_{\text{cr}}$ .

Figure 2 shows typical examples of stable SVs, as well as the amplitude and phase patterns of stable MMs, at different values of  $L$ . It is observed that the decrease of  $L$  makes the MM's shape more circular, which is a natural consequence of squeezing the mode by the spatial confinement. As concerns SVs, due to their axial symmetry they are displayed by means of the radial cross sections.

The critical size  $L_{\text{cr}}$  being the most essential characteristic of the present setting, we display its dependence on  $N$  and  $\gamma$  in Fig. 3. In particular, Fig. 3(a) shows comparison of the VA-predicted and numerically found curves  $L_{\text{cr}}(N)$

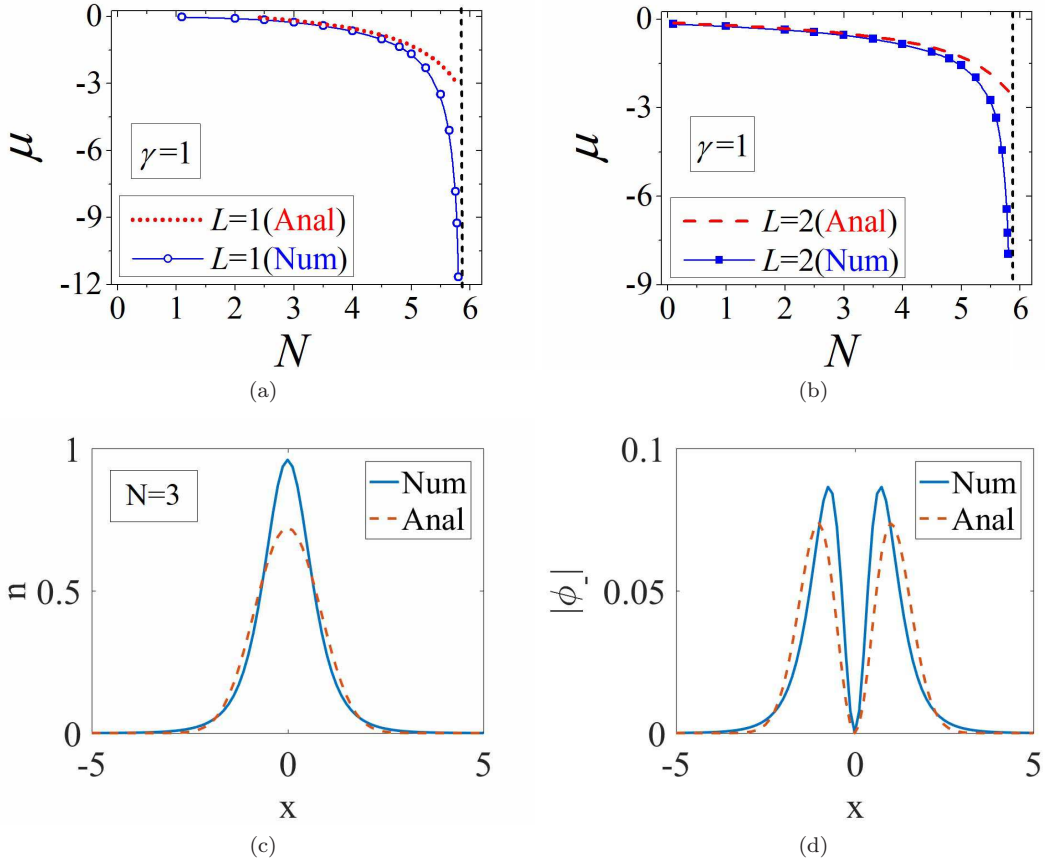


FIG. 4: (Color online) (a,b) Chemical potential  $\mu$  of the numerically generated (“Num”) SVs and MMs, as a function of  $N$ , for  $L = 1$  (a) and 2 (b), respectively, at  $\gamma = 1$  (the values of  $\mu$  fully coincide for the SVs and MMs). The red dot and dashed curves display the quasi-analytical (“Anal”) predictions of the VA for the same values,  $L = 1$  and 2, in panels (a) and (b), respectively, which are generated by Eqs. (12) and (13). (c,d) The comparison between the numerical result (the blue solid line) and the its VA counterpart (the red dashed line) for the cross section of the total density profile,  $n(\mathbf{r})$ , and the absolute value of the vortex component,  $|\phi_-(\mathbf{r})|$ , for the SV soliton with  $(N, \gamma, L) = (3, 1, 1)$ .

for SVs. The VA predicts  $L_{\text{cr}}(N)$  as the smallest value of  $L$  for which, with given  $N$ , numerical solution of variational equations (12) and (13) generates a meaningful solution for parameters  $A$ ,  $B$ , and  $W$ . It is seen that the agreement is reasonable, the numerically generated SVs being somewhat more robust, as  $L_{\text{cr}}$  is slightly smaller for them.

Further, the identical equality of the values of  $L_{\text{cr}}$  for SVs and MMs at  $\gamma = 1$ , observed in Fig. 3(a), is a straightforward corollary of Eq. (14): in the limit of  $L \rightarrow L_{\text{cr}}$ , the vortex terms in the MM vanish, and this soliton degenerates into a bound states of two Townes’ solitons, which gives rise to the expression for its norm obtained by means of rescaling (14) from  $N_T$ . Then,  $M_{\text{lim}}$  is identical to  $N_T$  in the case of  $\gamma = 1$ . Furthermore, the same argument suggests that, for equal values of  $L_{\text{cr}}$  and given  $\gamma$ , the respective limit values of  $N$ , at which  $L = L_{\text{cr}}$  is attained by the SVs and MMs are related similarly to Eq. (14):

$$N_{\text{lim}}^{(\text{MM})}(L_{\text{cr}}) = 2(1 + \gamma)^{-1} N_{\text{lim}}^{(\text{SV})}(L_{\text{cr}}), \quad (19)$$

which is corroborated by numerical data. It is worthy to note that, according to Eq. (19)  $L_{\text{cr}}$  for SVs and MMs with equal norms are different at  $\gamma \neq 1$ . In particular, in Fig. 3(b) we display the  $L_{\text{cr}}(\gamma)$  dependences for the two soliton species, which agree with the prediction of Eq. (19). This panel also shows that  $L_{\text{cr}}$  of both species decrease with the increase of  $\gamma$ .

The decrease of  $L_{\text{cr}}$  with the increase of  $N$  and  $\gamma$ , clearly seen in Fig. 3, is a natural trend, as the stronger nonlinearity, corresponding to larger  $N$  and/or  $\gamma$ , leads to self-compression of the solitons, making them less sensitive to the spatial confinement of the SO coupling. Inverting dependence  $L_{\text{cr}}(N)$ , displayed in Fig. 3(a), i.e., considering it as  $N(L)$ , one can interpret it in an alternative way: for given  $L$ , the SVs and MMs exist, severally, in regions

$$N_{\text{lim}}^{(\text{SV})}(L) < N < N_T, \quad N_{\text{lim}}^{(\text{MM})}(L) < N < 2(1 + \gamma)^{-1} N_T, \quad (20)$$

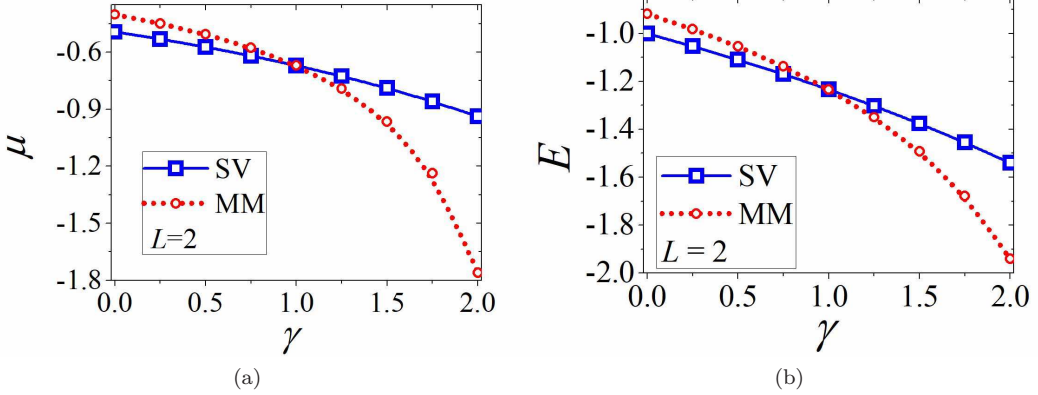


FIG. 5: (Color online) (a,b) The energy and chemical potential of SVs (blue solid with squares) and MMs (red dots with circles) vs.  $\gamma$  with  $(N,L) = (3.5, 2)$ . These two panels indicate that the SV and MM degenerate at  $\gamma = 1$ , the condition of a Manakov type. .

while in the case of  $L = \infty$  there is no lower norm threshold necessary for the existence of stable SVs and MMs [18].

Lastly, the fact that  $L_{\text{cr}}$ , i.e., the localization size of the wave functions, remains finite at  $N \rightarrow 0$  in Fig. 3(a) demonstrates that the spatially localized SO coupling plays the role of an effective trapping potential in the linear system. A similar effect was mentioned in Ref. [39], where a 1D localized potential was induced by a finite area of SO-coupling.

For fixed values of  $L$  and  $\gamma$ , soliton families are naturally characterized by dependences  $\mu(N)$ , which are displayed for  $L = 1$  and 2 with  $\gamma = 1$  in Fig. 4(a,b), respectively. An essential fact is that  $\mu(N)$  curves satisfy the Vakhitov-Kolokolov criterion,  $d\mu/dN < 0$ , which is a well-known necessary stability condition for the solitons [1, 2, 46]. Moreover, the comparison between the numerical results and the VA-predicted dependence  $\mu(N)$  for SVs, see Eq. (12), shows that they coincides very well for small values of  $N$ , deviating at larger  $N$ , the reason being that the simple ansatz (10) is not accurate enough for large norms. In addition, the comparison between typical numerically found shapes of the SV and the respective VA prediction is shown in Fig. 4(b,c), showing qualitative agreement.

## B. Stability of the 2D solitons

In Ref. [18] it was found that, in the uniform space ( $L = \infty$ ), the SVs and MMs are stable, respectively, at  $\gamma \geq 1$  and  $\gamma \geq 1$ , where they realize the ground state of the system, i.e., the energy minimum for given  $N$ . At  $\gamma > 1$ , the SVs, whose energy exceeds that of the MMs, are subject to weak instability, which sets them in spontaneous motion. Similarly, the MMs are unstable at  $\gamma < 1$ , where they tend to spontaneously rearrange into SVs, with lower energy.

In the present system, with  $L < \infty$ , the ground-state switch between SVs and MMs also happens. Fig. 5(a) shows the energies of the SVs and MMs with  $(N, L) = (3.5, 2)$  as a function of  $\gamma$ . It is seen that the SV and MM realize the energy minimum, which are always stable, at  $\gamma > 1$  and  $\gamma < 1$ , respectively. Their energies are equal to each other at  $\gamma = 1$ , which is the system of the Manakov's type [47]. For the comparison's sake,  $\mu(\gamma)$  curves for the same parameters are displayed in Fig. 5(b), showing that  $\mu_{\text{SV}} = \mu_{\text{MM}}$  point is also at  $\gamma = 1$ , in accordance with the above-mentioned degeneracy of the soliton families in this case, cf. Fig. 4(a). Note that both the ground states and ones different from them are produced here by the imaginary-time-integration method. In this connection, it is relevant to mention that non-ground states in SO-coupled systems were previously produced by means of the imaginary-time integration, provided that the input and integration procedure are subject to specific constraints, and the numerical algorithm is precise enough, to prevent a spontaneous transition to the ground states, see Refs. [11], [18], [34], and [48, 49].

Similar to the situation for  $L = \infty$ , explored in Ref. [18], the solitons which do not correspond to the energy minimum tend to become unstable. However, in the system with finite  $L$  the instability, which includes spontaneous drift of the solitons, may be partly suppressed by the confinement. To illustrate the results, Fig. 6 displays simulated evolution of the density profiles for unstable MMs at  $\gamma = 0$ , and unstable SVs at  $\gamma = 2$ , at different values of  $L$ . It is seen that their drift is indeed confined by the finite values of  $L$ . Actually, the confinement may effectively suppress the MM's instability, as seen in Fig. 6(c), or transform the MM into a robust a breather, see Fig. 6(b). For the SVs which do not correspond to the energy minimum, the instability remains conspicuous even in the presence of the relatively tight spatial confinement.

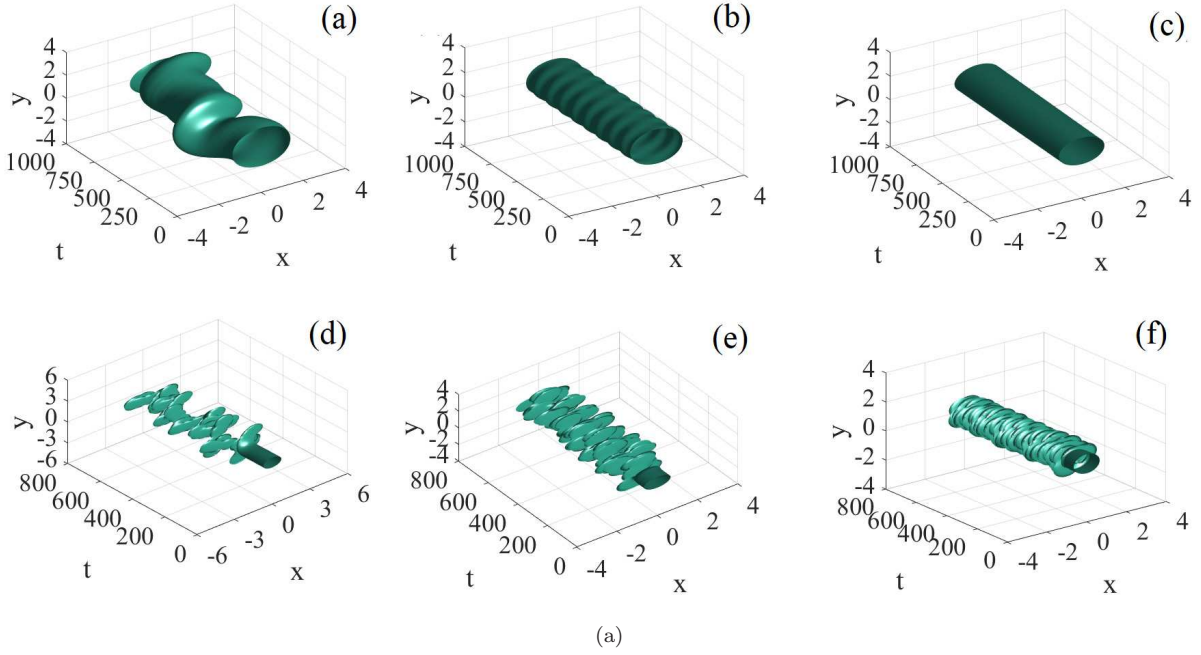


FIG. 6: (Color online) (a,b,c) Simulations of the perturbed evolution of unstable MMs (in the case when they do not represent the energy minimum), shown by means of the density profile,  $n(\mathbf{r}, t)$ , for  $(N, \gamma, L) = (3.5, 0, 20)$  (a),  $(3.5, 0, 10)$  (b), and  $(3.5, 0, 2)$  (c). (d,e,f) The same for unstable SVs, for  $(N, \gamma, L) = (3.5, 2, 10)$  (d),  $(3.5, 2, 5)$  (b) and  $(3.5, 2, 2)$  (f).

Lastly, in addition to the fundamental 2D solitons considered above, the SO-coupled system can also produce excited states [18, 48, 49], which are produced by adding the same vorticity,  $S \geq 1$ , to both components of the 2D soliton. In particular, excited states of SVs can be generated by input  $\phi_+^{(\text{SV})} = A_+ r^S \exp(-\alpha_+ r^2 + iS\theta)$ ,  $\phi_-^{(\text{SV})} = A_- r^S \exp(-\alpha_- r^2 + i(S+1)\theta)$ , where  $A_{\pm}$  and  $\alpha_{\pm} > 0$  are real constant. Numerical simulations demonstrate that all the excited states are unstable in the present model too.

## V. CONCLUSION

The objective of this work is to study the shapes and stability of 2D solitons of the SV (semi-vortex) and MM (mixed-mode) in the self-attractive pseudo-spinor BEC, with SO coupling applied in a confined area, following the analysis of effects of the spatial confinement in the 1D system [39]. Using numerical methods and the variational approximation, we have found that, with the decrease of the confinement radius,  $L$ , profiles shrink at first, and then expand to infinity (with the amplitude decaying to zero) when  $L$  approaches the critical value,  $L_{\text{cr}}$ , below which 2D solitons do not exist. The dependences of  $L_{\text{cr}}$  on the solitons' norm,  $N$ , and the relative strength of the cross-attraction,  $\gamma$ , are produced, on the basis of numerical results,  $L_{\text{cr}}$  being smaller for stronger nonlinearity, i.e., larger  $N$  and  $\gamma$ . In addition to the stability of the solitons which play the role of the ground state, i.e., SV at  $\gamma < 1$  and MM at  $\gamma > 1$ , unstable MMs (which do not represent the ground state) may be partly stabilized by the spatial confinement of the SO coupling.

As an extension of the present work, a challenging possibility is to address 3D solitons in the binary BEC with a spatially confined strength of the SO coupling, following the analysis for the 3D uniform space developed in Ref. [19].

## Acknowledgments

We appreciate valuable discussions with G. Jūzeliunas, Y. V. Kartashov, and V. V. Konotop, and assistance in numerical calculations provided by Hao Huang and Rongxuan Zhong. This work was supported, in part, by NNSFC (China) through grants No. 11575063, 61471123, 61575041, by the joint program in physics between NSF and Binational (US-Israel) Science Foundation through project No. 2015616, and by the Natural Science Foundation

of Guangdong Province, through grant No. 2015A030313639. B.A.M. appreciates a foreign-expert grant from the Guangdong province (China).

---

[1] L. Bergé, Wave collapse in physics: principles and applications to light and plasma waves, *Phys. Rep.* **303**, 259 (1998).

[2] C. Sulem and P. L. Sulem, *The nonlinear Schrödinger equation: self-focusing and wave collapse* (Springer: Berlin, 1999).

[3] F. Maucher, N. Henkel, M. Saffman, W. Krolikowski, S. Skupin, and T. Pohl, Rydberg-Induced Solitons: Three-Dimensional Self-Trapping of Matter Waves, *Phys. Rev. Lett.* **106**, 170401 (2011).

[4] P. Pedri and L. Santos, Two-Dimensional Bright Solitons in Dipolar Bose-Einstein Condensates, *Phys. Rev. Lett.* **95**, 200404 (2006).

[5] I. Tikhonenkov, B. A. Malomed, and A. Vardi, Anisotropic Solitons in Dipolar Bose-Einstein Condensates., *Phys. Rev. Lett.* **100**, 090406 (2008).

[6] X. Chen, Y. Chuang, C. Lin, C. Wu, Y. Li, B. A. Malomed, and R. Lee, Magic tilt angle for stabilizing two-dimensional solitons by dipole-dipole interactions, *Phys. Rev. A* **96**, 043631 (2017).

[7] J. Qin, G. Dong, and B. A. Malomed, Stable giant vortex annuli in microwave-coupled atomic condensates, *Phys. Rev. A* **94**, 053611 (2016).

[8] T. D. Lee, K. S. Huang, and C. N. Yang, Eigenvalues and eigenfunctions of a Bose system of hard spheres and Its Low-temperature properties, *Phys. Rev.* **106**, 1135(1957).

[9] D. S. Petrov, Quantum mechanical stabilization of a collapsing Bose-Bose mixture, *Phys. Rev. Lett.* **115**, 155302 (2015).

[10] D. S. Petrov and G. E. Astrakharchik, Ultradilute low-dimensional liquids, *Phys. Rev. Lett.* **117**, 100401 (2016).

[11] Y. Li, Z. Luo, Y. Liu, Z. Chen, C. Huang, S. Fu, H. Tan, and B. A. Malomed, Two-dimensional solitons and quantum droplets supported by competing self- and cross-interactions in spin-orbit-coupled condensates, *New J. Phys.* **19**, 113043 (2017).

[12] M. Schmitt, M. Wenzel, F. Böttcher, I. Ferrier-Barbut, and T. Pfau, Self-bound droplets of a dilute magnetic quantum liquid, *Nature* **539**, 259 (2016).

[13] I. Ferrier-Barbut, H. Kadau, M. Schmitt, M. Wenzel, and T. Pfau, Observation of quantum droplets in a strongly dipolar Bose gas, *Phys. Rev. Lett.* **116**, 215301 (2016).

[14] L. Chomaz, S. Baier, D. Petter, M. J. Mark, F. Wächtler, L. Santos, and F. Ferlaino, Quantum-fluctuation-driven crossover from a dilute Bose-Einstein condensate to a macrodroplet in a dipolar quantum fluid, *Phys. Rev. X* **6**, 041039 (2016).

[15] C. R. Cabrera, L. Tanzi, J. Sanz, B. Naylor, P. Thomas, P. Cheiney, and L. Tarruell, Quantum liquid droplets in a mixture of Bose-Einstein condensates, *Science* **359**, 301 (2018).

[16] P. Cheiney, C. R. Cabrera, J. Sanz, B. Naylor, L. Tanzi, and L. Tarruell, Bright soliton to quantum droplet transition in a mixture of Bose-Einstein condensates, *Phys. Rev. Lett.* **120**, 135301 (2018).

[17] G. Semeghini, G. Ferioli, L. Masi, C. Mazzinghi, L. Wolswijk, F. Minardi, M. Modugno, G. Modugno, M. Inguscio, and M. Fattori, Self-bound quantum droplets in atomic mixtures, arXiv:1710.10890.

[18] H. Sakaguchi, B. Li, and B. A. Malomed, Creation of two-dimensional composite solitons in spin-orbit-coupled self-attractive Bose-Einstein condensates in free space, *Phys. Rev. E* **89**, 032920 (2014).

[19] Y. Zhang, Z. Zhou, B. A. Malomed, and H. Pu, Stable Solitons in Three Dimensional Free Space without the Ground State: Self-Trapped Bose-Einstein Condensates with Spin-Orbit Coupling, *Phys. Rev. Lett.* **115**, 253902 (2015).

[20] Y. J. Lin, K. Jimenez-Garcia, and I. B. Spielman, Spin"Corbit-coupled Bose"CEinstein condensates, *Nature* **471**, 83 (2011).

[21] D. L. Campbell, G. Juzeliūnas, and I. B. Spielman, Realistic Rashba and Dresselhaus spin-orbit coupling for neutral atoms, *Phys. Rev. A* **84**, 025602 (2011).

[22] B. M. Anderson, G. Juzeliūnas, V. M. Galitski, and I. B. Spielman, Synthetic 3D spin-orbit coupling, *Phys. Rev. Lett.* **108**, 235301 (2012).

[23] V. Galitski and I. B. Spielman, Spin"Corbit coupling in quantum gases, *Nature* **494**, 49 (2013).

[24] N. Goldman, G. Juzeliunas, P. Öhberg, and I. B. Spielman, Light-induced gauge fields for ultracold atoms, *Rep. Progr. Phys.* **77**, 126401 (2014).

[25] H. Zhai, Degenerate quantum gases with spin"Corbit coupling: a review, *Rep. Prog. Phys.* **78**, 026001 (2015).

[26] Z. Wu, L. Zhang, W. Sun, X.-T. Xu, B.-Z. Wang, S.-C. Ji, Y. Deng, S. Chen, X.-J. Liu, and J.-W. Pan, *Science* **354**, 83 (2016).

[27] Huang, Z. Meng, P. Wang, P. Peng, S. Zhang, L. Chen, D. Li, Q. Zhou and J. Zhang, Experimental realization of two-dimensional synthetic spinCorbit coupling in ultracold Fermi gases, *Nat. Phys.* **12**, 540 (2016).

[28] G. Dresselhaus, Spin-orbit coupling effects in zinc blende structures, *Phys. Rev.* **100**, 580 (1955).

[29] H. Sakaguchi, E. Ya. Sherman, and B. A. Malomed, Vortex solitons in two-dimensional spin-orbit coupled Bose-Einstein condensates: Effects of the Rashba-Dresselhaus coupling and the Zeeman splitting, *Phys. Rev. E* **94**, 032202 (2016); H. Sakaguchi, B. Li, E. Ya. Sherman, and B. A. Malomed, *Romanian Rep. Phys.* **70**, 502 (2018).

[30] J. Dias, M. Figueira, V. V. Konotop, Coupled nonlinear Schrödinger equations with a gauge potential: Existence and blowup, *Stud. Appl. Mat.* **136**, 241 (2015).

[31] Sh. Mardonov, E. Ya. Sherman, J. G. Muga, H.-W. Wang, Y. Ban, and X. Chen, Collapse of spin-orbit-coupled Bose-Einstein condensates, *Phys. Rev. A* **91**, 043604 (2015).

- [32] Y. Zhang, M. E. Mossman, T. Busch, P. Engels, and C. Zhang, Properties of spin-orbit-coupled Bose-Einstein condensates, *Front. Phys.* **11**, 118103 (2016).
- [33] Y. V. Kartashov, B. A. Malomed, V. V. Konotop, V. E. Lobanov, and L. Torner, Stabilization of solitons in bulk Kerr media by dispersive coupling, *Opt. Lett.* **40**, 1045(2015). Y. V. Kartashov, V. V. Konotop , and B. A. Malomed, Dark solitons in dual-core waveguides with dispersive coupling, *Opt. Lett.* **40**, 4126(2015).
- [34] H. Sakaguchi and B. A. Malomed, One- and two-dimensional solitons in  $\mathcal{PT}$ -symmetric systems emulating spin-orbit coupling, *New J. Phys.* **18** 105005 (2016).
- [35] Y. Xu, Y. Zhang, and C. Zhang, Bright solitons in a two-dimensional spin-orbit-coupled dipolar Bose-Einstein condensate, *Phys. Rev. A* **92**, 013633 (2015).
- [36] X. Jiang, Z. Fan, Z. Chen, W. Pang, Y. Li and B. A. Malomed, Two-dimensional solitons in dipolar Bose-Einstein condensates with spin-orbit coupling, *Phys. Rev. A* **93**, 023633 (2016); B. Liao, S. Li, C. Huang, Z. Luo, W. Pang, H. Tan, B. A. Malomed, and Y. Li, Anisotropic semivortices in dipolar spinor condensates controlled by Zeeman splitting, *Phys. Rev. A* **96**, 043613 (2017).
- [37] Y. Li, Y. Liu, Z. Fan, W. Pang, S. Fu, and B. A. Malomed, Two-dimensional dipolar gap solitons in free space with spin-orbit coupling, *Phys. Rev. A* **95**, 063613 (2017).
- [38] H. Sakaguchi, B. A. Malomed, One- and two-dimensional gap solitons in spin-orbit coupled systems with Zeeman splitting, *Phys. Rev. A* **97**, 013607 (2018).
- [39] Y. V. Kartashov, V. V. Konotop, and D. A. Zezyulin, Bose-Einstein condensates with localized spin-orbit coupling: Soliton complexes and spinor dynamics, *Phys. Rev. A* **90**, 063621 (2014).
- [40] K. E. Strecker, G. B. Partridge, A. G. Truscott, and R. G. Hulet, *Nature* **417**, 150 (2002).
- [41] L. Khaykovich, F. Schreck, G. Ferrari, T. Bourdel, J. Cubizolles, L. D. Carr, Y. Castin, and C. Salomon, *Science* **296**, 1290 (2002).
- [42] S. L. Cornish, S. T. Thompson, and C. E. Wieman, *Phys. Rev. Lett.* **96**, 170401 (2006).
- [43] L. Salasnich, Bright solitons in ultracold atoms, *Opt. Quant. Electron.* **49**, 409 (2017).
- [44] R. Y. Chiao, E. Garmire, and C. H. Townes, Self-trapping of optical beams, *Phys. Rev. Lett.* **13**, 479-482 (1964).
- [45] M. Desaix, D. Anderson, and M. Lisak, 1991, Variational approach to collapse of optical pulses, *J. Opt. Soc. Am. B* **8**, 2082-2086 (1991).
- [46] M. Vakhitov and A. Kolokolov, Stationary solutions of the wave equation in a medium with nonlinearity saturation, *Radiophys. Quantum Electron.* **16**, 783-789 (1973).
- [47] D. J. Kaup and B. A. Malomed, Soliton trapping and Daughter Waves in the Manakov model, *Phys. Rev. A* **48**, 599 (1993).
- [48] C. Huang, Y. Ye, S. Liu, H. He, W. Pang, B. A. Malomed, Y. Li, Excited states of two-dimensional solitons supported by spin-orbit coupling and field-induced dipole-dipole repulsion, *Phys. Rev. A* **97**, 013636 (2018).
- [49] R. Zhong, Z. Chen, C. Huang, Z. Luo, H. Tan, B. A. Malomed, Y. Li, Self-trapping under the two-dimensional spin-orbit-coupling and spatially growing repulsive nonlinearity, *Front. Phys.* **13**, 130311 (2018).